Electronic Supplementary Material (ESI) for Physical Chemistry Chemical Physics.

Electronic Supporting Information for

Structural insights into the multinuclear speciation of tetravalent cerium in the tri-*n*-butyl phosphate–*n*-dodecane solvent extraction system

Mark R. Antonio,[1,*] Ross J. Ellis[1,‡], Shanna L. Estes[1], and Mrinal K. Bera[1,§]

[1]Chemical Sciences and Engineering Division, Argonne National Laboratory, Argonne, IL 60439 U.S.A. mantonio@anl.gov

Present addresses: [§]Center for Advanced Radiation Sources, The University of Chicago, Argonne, IL 60439 U.S.A.; [‡]Borregaard, 1701 Sarpsborg, Norway

Table S1. EXAFS results for the aqueous, initial 0.04 M Ce(IV) solution in 3 M HNO_3 from fitting with three different models involving three (O, O, O), four (O, O, O, O), and five (O, O, O, O, Ce) coordination spheres.[a] Values without error bars indicate fixed parameters. The error bars (in parentheses) on the refined variables are shown at the 3σ level. The double prime entries indicate that the parameter was linked to the one in the row above. Fit indices (F) decrease showing statistically relevant improvements in modeling with the addition of shells as evaluated in the manner described elsewhere.[1]

Shell	**r, Å**	**CN**	**σ^2, Å^2**	**ΔE_0, eV**
Three-shell model – F = 70.0				
O(1)	2.48(1)	5.7(7)	0.007(2)	-1.7(9)
O(2)	3.23(6)	1.0(9)	″	″
O(3)	3.84(3)	3.7(10)	″	″
Four-shell model – F = 65.9				
O(0)	2.03(7)	0.3(1)	0.008(2)	-1.6(9)
O(1)	2.48(1)	5.9(9)	″	″
O(2)	3.23(6)	1.1(8)	″	″
O(3)	3.84(3)	3.9(11)	″	″
Five-shell model – F = 64.3				
O(0)	2.03(8)	0.3(1)	0.008(2)	-1.7(9)
O(1)	2.48(1)	6.0(10)	″	″
O(2)	3.23(6)	1.2(8)	″	″
O(3)	3.84(3)	3.7(12)	″	″
Ce	4.04(8)	0.4(2)	″	″

[a] In the three-shell model, the first shell, O(1), is attributed to backscattering from the O atoms of water and nitrate anions (monodentate and bidentate bonding); the second shell, O(2), is attributed to either N atoms of the nitrate anions and/or O atoms of water and nitrate; the

third shell, O(3), arises from distant O atoms that are presumably associated with nitrate anions and/or hydrogen-bonded water. The four-shell model contains a short bridging O interaction, O(0), in addition to the same backscattering atoms of the three-shell model. The five-shell model is like the four-shell model but with the addition of a distant Ce-Ce interaction.

Table S2: Fitting parameters for the SAXS (Figure 7(a) of the article text and ESI, Figure S8) of the organic, equilibrium phases from the Baxter sticky sphere modeling that is illustrated in Figure 7(b) of the article text and described in detail elsewhere.[2] The estimated standard deviations at the 3-sigma level are shown.

Phase	**Rc,[a] Å**	**ρ_c,[b] e^-/Å^3**	**Rs,[a] Å**	**b_{Rc+Rs}[c]**	**ρ_s,[b] e^-/Å^3**	**η,[d] %**	**τ[e]**	**N[f] ($\times10^{-4}$)**	**U,[g] k_BT**
$I_{b,H2O}$[h] (P1x)	2.76±0.71	0.084±0.062	5.57±0.77	6.66±0.02	-0.003±0.014	4.09±37	0.121±0.46	6.028±1.00	-4.3±1.2
$I_{b,HNO3}$[i] (P3o)	2.76±0.49	0.088±0.044	5.59±0.44	1.25±0.55	0.0009±0.001	2.1±1.7	0.069±0.022	4.91±3.77	-4.8±1.1
$I_{b,org,eq}$[j] (P1o)	2.85±0.36	0.085±0.028	6.08±0.33	1.17±0.28	0.0008±0.0008	1.8±1.2	0.066±0.024	4.04±2.08	-4.8±0.8
$I_{t,org,eq}$[k] (P2o)	2.84±0.03	0.078±0.018	6.32±0.24	1.20±0.25	0.0009±0.0006	1.6±1.3	0.068±0.030	4.73±1.67	-4.8±0.6
$d_{t,org,eq}$[l] (P2t)	3.17±0.08	0.103±0.006	6.49±0.08	1.28±0.12	0.0019±0.0005	32.5±3.2	0.413±0.12	32.0±4.0	-3.0±0.1

[a] The radii of the inner, hydrophilic (polar) cores, Rc, of the spherical reverse micelles whose interactions are described with Baxter's sticky sphere model, in which the reverse micelles exhibit an average interparticle separation, Rs. In other words, Rs is the mean value of the "hard" sphere radius of the micelles. [b] ρ_c and ρ_s are the average electron densities of the reverse micelle core and corona, respectively. The values are given with respect to the electron density of the bulk organic phase of *n*-dodecane. The ρ_c values are large because the core contains electron-rich Ce(IV) ions (Z = 58) that provide strong contrast with the low-Z, *n*-dodecane solvent. In contrast, the ρ_s values are low because the *n*-butyl groups of TBP in the corona are essentially equivalent to the $-CH_2-$ chains of the *n*-dodecane solvent. [c] A measure of reverse micelle polydispersity using Weibull distribution, for which values smaller than 1 mean a monotonic distribution of micelles without any preferable size and larger than 1 mean the micelles have a preferable size.[3] [d] The

reverse micelle volume fraction. [e] The dimensionless stickiness parameter. [f] A measure of relative number of reverse micelles in the scattering volume. [g] The micelle-micelle interaction energy, also the depth of the potential well. [h] Organic, equilibrium solution from biphasic LLE of H_2O (without Ce). [i] Organic, equilibrium solution from biphasic LLE of 3 M HNO_3 (without Ce). [j] Organic, equilibrium solution from biphasic LLE of 0.04 M Ce^{4+} in 3 M HNO_3 (abbreviated $l_{b,org,eq}$, see Figure 1(a) of the article text). [k] Light, organic, equilibrium solution from triphasic LLE of 0.40 M Ce^{4+} in 3 M HNO_3 (abbreviated $l_{t,org,eq}$, see Figure 1(b) of the article text). [l] Dense organic, equilibrium solution (third phase) from triphasic LLE of 0.40 M Ce^{4+} in 3 M HNO_3 (abbreviated $d_{t,org,eq}$, see Figure 1(b) of the article text).

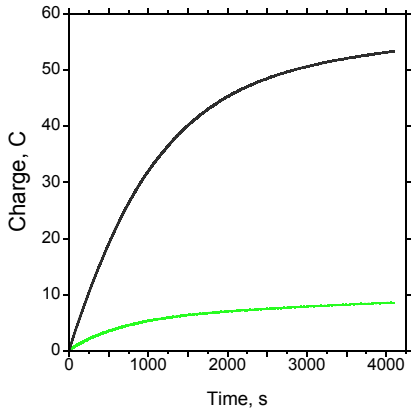

Figure S1. Chronocoulometry data for the electrolysis of the two 3 M HNO_3 solutions with $Ce(NO_3)_3$ concentrations of 0.04 and 0.40 M (green and black lines, respectively). Complete oxidation to Ce(IV) was achieved in 68 minutes.

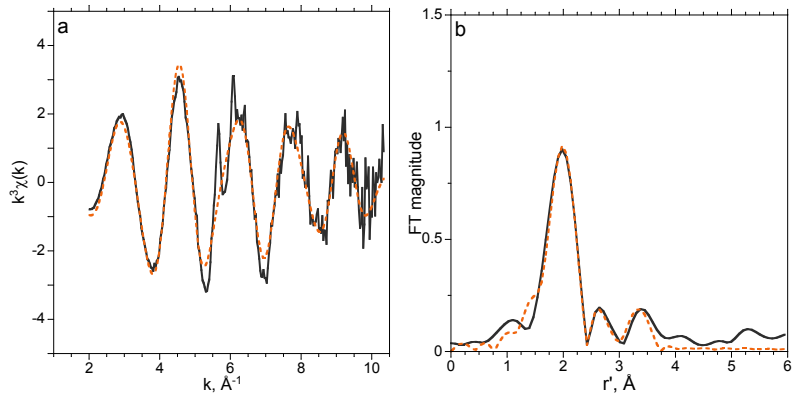

Figure S2. (a) The $k^3\chi(k)$ EXAFS for the aqueous, initial phase of 0.04 M Ce(IV) in 3 M HNO_3 from experiment (solid black line) compared with the fit (dashed orange line) using the three-shell (O, O, O) model. (b) The corresponding FT data, which are uncorrected for phase shift (r') as shown, of the experimental data (solid black line) and of the fitted data (dashed orange line).

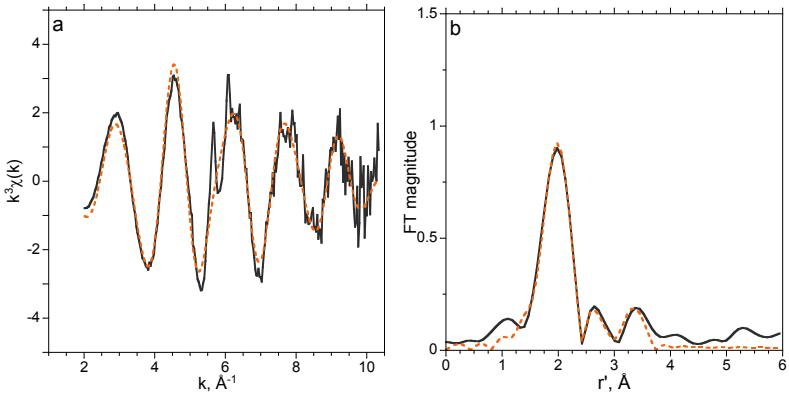

Figure S3. (a) The $k^3\chi(k)$ EXAFS for the aqueous, initial phase of 0.04 M Ce(IV) in 3 M HNO_3 from experiment (solid black line) compared with the fit (dashed orange line) using the four-shell (O, O, O, O) model. (b) The corresponding FT data, which are uncorrected for phase shift (r') as shown, of the experimental data (solid black line) and of the fitted data (dashed orange line).

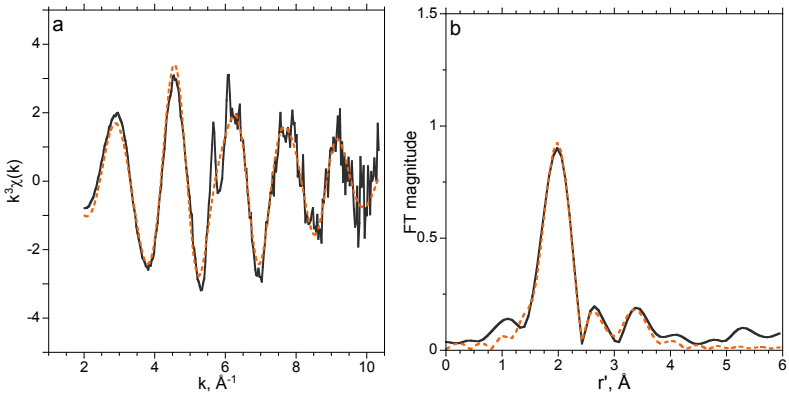

Figure S4. (a) The $k^3\chi(k)$ EXAFS for the aqueous, initial phase of 0.04 M Ce(IV) in 3 M HNO_3 from experiment (solid black line) compared with the fit (dashed orange line) using the five-shell (O, O, O, O, Ce) model. (b) The corresponding FT data, which are uncorrected for phase shift (r') as shown, of the experimental data (solid black line) and of the fitted data (dashed orange line).

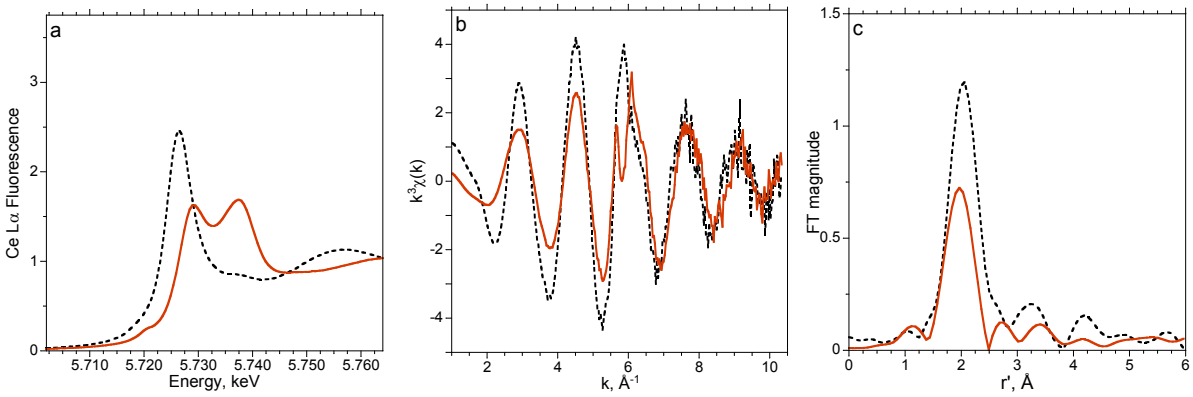

Figure S5. (a) Ce L_3-edge XANES data for the aqueous, initial phase of 0.40 M $Ce(NO_3)_3 \cdot 6H_2O$ in 3 M HNO_3 (black dashed line) and the electrolyzed Ce(IV) solution (orange line) and (b) the corresponding $k^3\chi(k)$ EXAFS and (c) Fourier transform data.

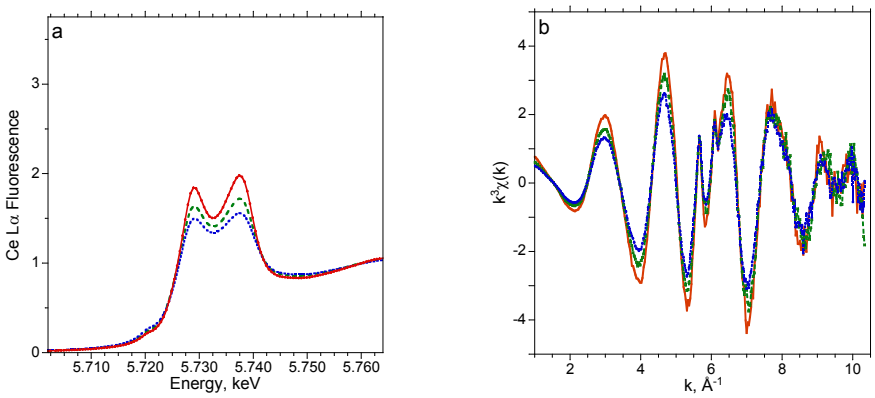

Figure S6. (a) Ce L_3-edge XANES data for the light (green dashed line) and dense (blue dotted line) organic, equilibrium solutions from the triphasic LLE system ($l_{t,org,eq}$ and $d_{t,org,eq}$, respectively, Figure 1(b)) as well as the organic, equilibrium solution from the biphasic LLE system (red line, $l_{b,org,eq}$ of Figure 1(a)); (b) the corresponding $k^3\chi(k)$ EXAFS data. The diminution of signal intensities noted with increasing Ce(IV) concentrations (0.04 M for $l_{b,org,eq}$, 0.136 M for $l_{t,org,eq}$, and 1.47 M for $d_{t,org,eq}$, see Table 5 of the article text) is due to effects of self-absorption, which do not vitiate the comparison of peak positions and phases.

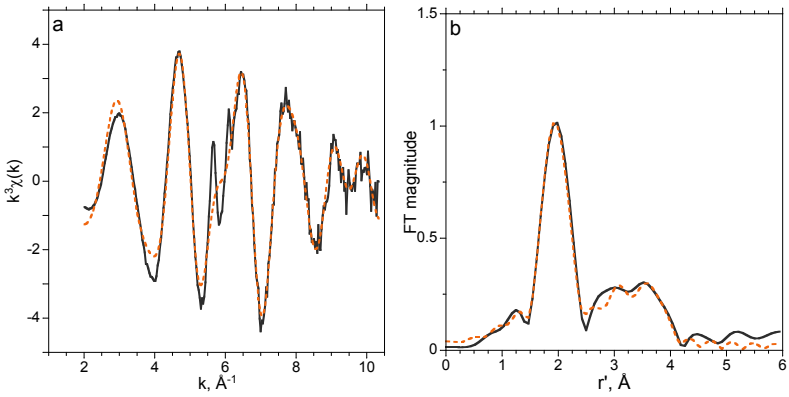

Figure S7. (a) The $k^3\chi(k)$ EXAFS for the organic, equilibrium phase from LLE of 0.04 M Ce(IV) in 3 M HNO_3 with 20 % TBP in *n*-dodecane (Figure 1(a) of the article text) from experiment (solid black line) compared with the fit (dashed orange line) using the six-shell (O, O, N, P, Ce, O) model. (b) The corresponding FT data, which are uncorrected for phase shift (r') as shown, of the experimental data (solid black line) and of the fitted data (dashed orange line). The metrical parameters are provided in Table 4 of the article text.

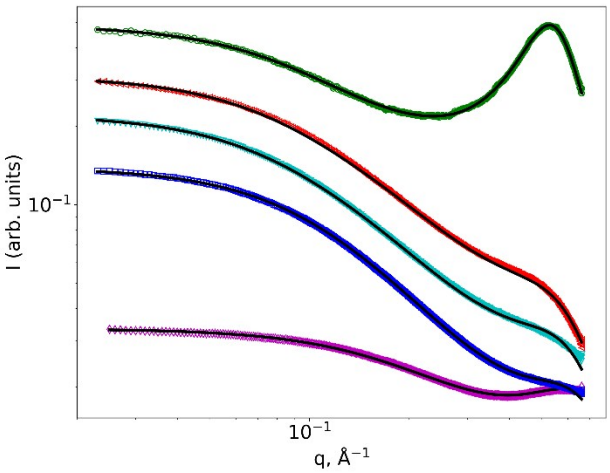

Figure S8. SAXS data for five organic, equilibrium solutions after LLE. Working up from the bottom, the data for the organic, equilibrium phase after contact with water (without Ce) are shown as the magenta line. It reveals a response that is typical of particle scattering, in this case by TBP oligomers, principally dimers.[4-11] The blue response is for the organic, equilibrium phase following contact with 3 M HNO_3 (still without Ce). The contrast is greatly increased from the water-contacted organic phase due to the uptake of nitric acid (and water) as reverse micellar TBP acid hydrates. The solute concentrations in the two aforementioned organic, equilibrium phases are provided in Table S3 below. The contrast continues to increase (cyan line) as Ce(IV) is incorporated into the organic, equilibrium phase after contact with 0.04 M Ce(IV) in 3 M HNO_3. The extraction of 0.40 M Ce(IV) in 3 M HNO_3, produces two organic, equilibrium phases: (1) owing to the increased Ce concentration, the light organic phase (red line) has more contrast than the corresponding organic phase from the extraction of a 10-fold more dilute solution of Ce(IV). (2) The third phase (green line) exhibits the highest contrast due to the high-concentrations of solutes H_2O, HNO_3, TBP, and Ce(IV), see Table 5 in the article text. The SAXS for the third phase

reveals a broad and resolved peak at approx. 0.53 $Å^{-1}$, due to the presence of correlated structures in the third phase liquid, namely between Ce-bearing reverse micelles. The black lines illustrate the fits using the Baxter model; the parameters are provided in Table S2.

Table S3. Concentrations (M) of solutes in the *n*-dodecane phases with 20% TBP after LLE of water and nitric acid (both without cerium).

Aqueous, initial	**Organic, equilibrium**	**$[HNO_3]_{org}$**	**$[H_2O]_{org}$**	**$[TBP]_{org}$**
H_2O	Light, biphasic, $l_{b,H2O}$	0	0.24	0.73
3 M HNO_3	Light, biphasic, $l_{b,HNO3}$	0.45	0.48	0.73

References

1. M. R. Antonio, J. Jing, B. P. Burton-Pye and L. C. Francesconi, *Dalton Trans.*, 2010, **39**, 7980-7992.
2. M. K. Bera, R. J. Ellis, B. P. Burton-Pye and M. R. Antonio, *Phys. Chem. Chem. Phys.*, 2014, **16**, 22566-22574.
3. P. Calandra, A. Longo and V. T. Liveri, *J. Phys. Chem. B*, 2003, **107**, 25-30.
4. R. Motokawa, S. Suzuki, H. Ogawa, M. R. Antonio and T. Yaita, *J. Phys. Chem. B*, 2012, **116**, 1319-1327.
5. A. G. Baldwin, N. J. Bridges and J. C. Braley, *Ind. Eng. Chem.*, 2016, **55**, 13114-13119.
6. A. G. Baldwin, Y. Yang, N. J. Bridges and J. C. Braley, *J. Phys. Chem. B*, 2016, **120**, 12184-12192.
7. M. J. Servis, C. A. Tormey, D. T. Wu and J. C. Braley, *J. Phys. Chem. B*, 2016, **120**, 2796-2806.
8. Q. N. Vo, L. X. Dang, M. Nilsson and H. D. Nguyen, *J. Phys. Chem. B*, 2016, **120**, 6985-6994.
9. Q. N. Vo, C. A. Hawkins, L. X. Dang, M. Nilsson and H. D. Nguyen, *J. Phys. Chem. B*, 2015, **119**, 1588-1597.
10. Q. N. Vo, J. L. Unangst, H. D. Nguyen and M. Nilsson, *J. Phys. Chem. B*, 2016, **120**, 6976-6984.
11. A. Mondal and S. Balasubramanian, *Curr. Sci.*, 2014, **106**, 1235-1242.